Eur. Phys. J. A (2025) 61:158
https://doi.org/10.1140/epja/s10050-025-01634-1

THE EUROPEAN PHYSICAL JOURNAL A

Regular Article - Experimental Physics

Decay properties of the fission isomer ^{236m}U

P. Reiter[1,a], **D. Habs**[2], **D. Schwalm**[3], **P. G. Thirolf**[2]

[1] Institut für Kernphysik, Universität zu Köln, 50937 Köln, Germany
[2] Ludwig-Maximilians-Universität München, 85748 Garching, Germany
[3] Max-Planck-Institut für Kernphysik, Saupfercheckweg 1, 69117 Heidelberg, Germany

Received: 22 May 2025 / Accepted: 29 June 2025

Communicated by Silvia Leoni

Abstract The delayed γ decay and delayed fission of the shape isomer ^{236m}U were measured using the Heidelberg-Darmstadt Crystal Ball spectrometer. It is demonstrated that the isomeric γ decay and the delayed fission represent two competing decay channels of the same isomeric state. This conclusion is supported by four independent observations: (i) the measured half-lives of the delayed γ decay and delayed fission are identical, (ii) the excitation energy of the isomer is the same for both decay pathways, (iii) the missing energy in the prompt energy balance is equal for both decays, and (iv) the prompt energy spectra populating the second minimum are in agreement. An improved statistical analysis of the γ decay indicates that the excitation energy of the isomeric ground state in the second minimum is 2814 ± 33 keV. The γ back decay proceeds through several cascades involving known 1^- states of the normally deformed ^{236}U. A direct single-step γ transition is excluded within the experimental sensitivity.

1 Introduction

Fission or shape isomers in the actinide region have been extensively studied, revealing a variety of superdeformed nuclear states with axis ratios of approximately 2:1, particularly in nuclei ranging from uranium to berkelium. These isomeric states are generally associated with a second minimum in the potential energy surface of the fission barrier. Experimentally, their most well-established decay mode is delayed fission, corresponding to tunneling through the outer barrier. However, the observation of γ-decay from the second (superdeformed) minimum to the first (normally deformed) minimum – providing direct spectroscopic access to these states – has remained an enduring experimental challenge. Only in a few light actinide isotopes, such as ^{236}U [1] and ^{238}U [2], has this decay channel been observed.

Fission isomers were first identified by Polikanov [3], and their existence was later explained by Strutinsky [4], who introduced shell corrections to the macroscopic liquid-drop model. These corrections account for deviations in the single-particle level density as a function of nuclear deformation, leading to local minima in the potential energy surface. Although relatively small in magnitude, these shell effects can rival the difference between Coulomb and surface energies, stabilizing the superdeformed configurations.

The macroscopic-microscopic shell correction method has proven highly successful in describing the formation and properties of fission isomers [5]. Metag [6] provided an empirical framework linking the partial half-lives of isomeric fission to the fissility parameter $X = Z^2/A$, neutron number, curvature parameters, and specialization energies, reproducing experimental lifetimes within a factor of three. More recent theoretical advancements have further refined these models [7–9].

Figure 1 illustrates the typical double-humped fission barrier, where the first and second minima arise from the interplay of the macroscopic droplet model and microscopic shell effects. For states residing in the second minimum, both γ-decay to the ground state and fission through the outer barrier are quantum mechanically hindered. The associated tunneling probabilities are sensitive to the height and width of the respective barriers, as well as to the excitation energy of the isomeric state.

Spectroscopic studies of γ-ray transitions from superdeformed states – particularly rotational transitions – have enabled the extraction of moments of inertia, confirming the presence of the second minimum on a model-dependent basis [10]. Independent confirmation of the superdeformed character has been achieved via measurements of quadrupole

Deceased: D. Habs, D. Schwalm.

[a] e-mail: preiter@ikp.uni-koeln.de (corresponding author)

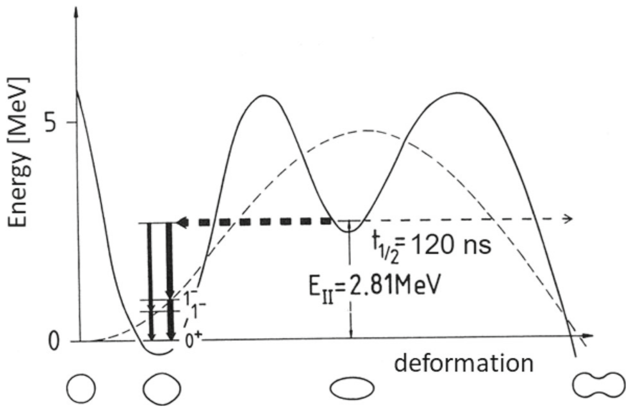

Fig. 1 Schematic representation of the double-humped fission barrier for ^{236}U, illustrating the inner and outer barrier and the superdeformed second minimum

moments, which are consistent with a semi-axis ratio of approximately 2:1 [11], providing direct evidence for the classification of these states as shape isomers. In recent years, improved experimental techniques have yielded a rich set of spectroscopic data for both the second and third minima in the potential energy surfaces of actinide nuclei; a comprehensive review can be found in Ref. [12].

The fission isomer in ^{236}U was first discovered in the early 1970s and has since been investigated using a variety of reactions, including photonuclear processes, thermal neutron capture, and (d,p) and (d,pn) reactions on ^{235}U and ^{236}U targets [13–16]. The isomeric state $^{236\mathrm{m}}$U has a reported half-life of approximately 120 ns. Experimental measurements of this half-life tend to cluster around two distinct values: one near 70 ns and another around 120 ns. The nuclear data evaluation in Ref. [17] adopts the shorter value, motivated by the interpretation in Ref. [18], which suggests that longer measured lifetimes may include contributions from higher-lying states. Nonetheless, the majority of experimental determinations favour the longer half-life near 120 ns. Early evidence for a rotational band built upon this state was reported in 1977 by Borggreen et al. [19]. Multiple efforts were undertaken to observe the γ-decay branch of this isomer [20,21]; however, clear identification was not achieved until the study by Schirmer et al. [1], which provided the first unambiguous evidence for this rare decay mode.

To investigate the extremely rare decays of shape isomers via delayed emission of radiation, a novel experimental approach was employed based on a calorimetric measurement of the complete energy balance in selected nuclear reactions by Schirmer et al. [1]. This was achieved using highly efficient and sensitive charged-particle and γ-ray detectors. The Heidelberg-Darmstadt Crystal Ball spectrometer, with its nearly 4π solid angle coverage provided by 162 independent NaI detectors, played a central role in enabling such measurements. Its excellent efficiency and timing resolution allowed for the detection not only of individual γ transitions but also of the total energy sum of both prompt and delayed γ-ray cascades.

Using this setup, compelling evidence was obtained for the very rare gamma decay of the shape isomer $^{236\mathrm{m}}$U. To further substantiate these findings and resolve remaining open questions, an additional measurement was carried out. The goal was to unambiguously link the observed delayed γ emission to the decay of the fission isomer $^{236\mathrm{m}}$U. For this purpose, the experimental configuration was extended by incorporating a dedicated fission-fragment detection system inside the spherical shell of the Crystal Ball spectrometer. Specifically, a hemispherical array of six independent parallel-plate avalanche counters (PPACs) was installed to detect fragments from the alternative decay channel of $^{236\mathrm{m}}$U via delayed fission. This configuration enables a definitive correlation between the observed isomeric γ decay and the decay of the $^{236\mathrm{m}}$U shape isomer.

The structure of this paper is as follows. Section 2 describes the experimental setup and measurement procedure, including subsections on calibration, efficiency determinations, and data analysis techniques. Section 3 presents the observation of the fission isomer in $^{236\mathrm{m}}$U. The subsequent Sect. 4 focuses on the isomeric γ decay following the ^{235}U(d,p) reaction. It is divided into two parts: the first addresses the 4^- K-isomer in ^{236}U, while the second discusses the γ decay of the shape isomer $^{236\mathrm{m}}$U. Common properties shared between the fission isomer and the γ decay of the shape isomer are examined in Sect. 5. Section 6 details the γ-decay cascades of the shape isomer $^{236\mathrm{m}}$U. Section 7 investigates two key branching ratios associated with the distinct decay modes of the isomer. Finally, Sect. 8 offers a summary and concluding remarks.

2 Detector setup and experiment

To study the rare decay channels of the shape isomer ^{236m}U via delayed γ emission and fission, the Heidelberg-Darmstadt Crystal Ball (CB) spectrometer [22] was adapted with additional detectors installed inside its spherical array. The CB, comprising 162 NaI detectors forming a 20 cm thick shell (with 159 active modules in this configuration), encloses a 50 cm diameter central chamber, achieving a 96% 4π solid angle coverage. Its granularity and timing resolution ($\Delta t_{CB} \approx 4.8$ ns) allow precise measurement of total energy, multiplicity, angular distributions, and timing of cascade decays.

A set of six parallel plate avalanche counters (PPACs), arranged hemispherically and spanning 30°–87° relative to the beam direction, was installed inside the CB to detect fission fragments, achieving 78% coverage per fragment pair. PPACs, operated with isobutane at 4.8 mbar and 490 V,

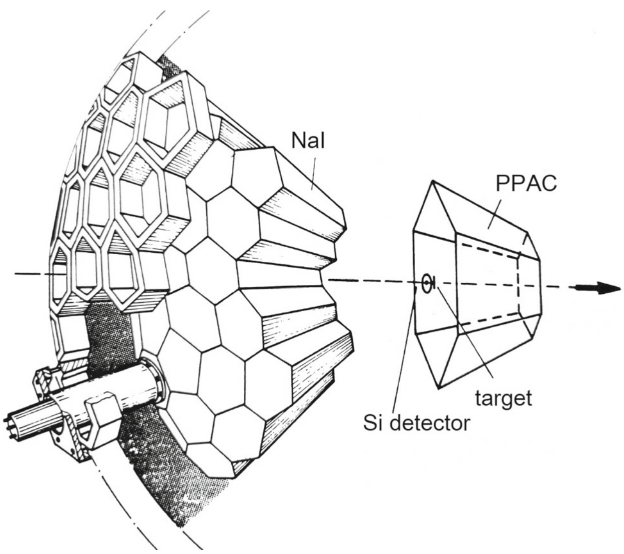

Fig. 2 Schematic of the experimental setup showing a segment of the Crystal Ball spectrometer, six PPACs at forward angles for fission fragment detection, and the annular Si detector at backward angles near the target for light charged particles

offered ∼ 4 ns time and sub-3 mm position resolution. A 450 mm^2 annular Si surface barrier detector, positioned 6.5 mm from the target at backward angles ($\theta = 119°–159°$, $\Delta\Omega = 23\%$), detected light charged particles, mainly protons, from (d,p) reactions. The detector was cooled to −15°C and shielded from fission fragments using a 40 µm polycarbonate foil and tantalum collimation (Fig. 2).

The experiment was conducted at the Max Planck Institute's Tandem accelerator with a pulsed 11 MeV deuteron beam (298 ns period, < 20 ns pulse width, 0.6–0.7 nA current). The ^{235}U target (3.5 mg/cm^2, 93% enriched) was prepared and mounted under inert conditions to prevent oxidation, and maintained in vacuum ($\leq 5 \times 10^{-6}$ mbar) during the 384-h measurement.

To suppress the dominant prompt reactions, a multi-level trigger system was implemented. All triggers required a prompt Si signal relative to the beam. Type 1 (prompt γ) required a prompt Si–CB coincidence and was downscaled 32:1. Type 2 (delayed γ) added a delayed CB hit (40–200 ns). Type 3 (prompt fission) required a Si–CB–PPAC coincidence within 60 ns. Type 4 (delayed fission) required a delayed PPAC hit (45–285 ns window) following a Si–CB prompt signal. Event digitization used CAMAC electronics, with data read by a VAX11/750 system. Trigger and detector rates were continuously monitored (Table 1).

2.1 Calibration and efficiency measurements

Energy calibration of the NaI detectors was performed using γ-ray sources of ^{152}Eu, ^{207}Bi, ^{88}Y, and ^{24}Na, covering energies up to 2.75 MeV. The time alignment of individual Crystal Ball modules was verified using the prompt γ peak (FWHM ≤ 5 ns) in the time difference between NaI and Si detector signals, enabling discrimination between prompt and delayed events.

Table 1 Count rates of detectors and trigger types of data acquisition, data volume recorded for different event types

Detector	Count rate	# events
Si ring detector	8.3 kHz	
PPAC (6 detectors)	1.4 kHz	
Crystal ball (159 detectors)	230 kHz	
All trigger	200 Hz	$2.8 \cdot 10^8$
Type 1 Si $\wedge$ CB$_{pro}$	22 Hz	$3.1 \cdot 10^7$
Type 2 Si $\wedge$ CB$_{pro}$ $\wedge$ CB$_{del}$	128 Hz	$1.8 \cdot 10^8$
Type 3 Si $\wedge$ CB$_{pro}$ $\wedge$ PPAC	52 Hz	$7.0 \cdot 10^7$
Type 4 Si $\wedge$ CB$_{pro}$ $\wedge$ PPAC$_{del}$	≤ 0.002 Hz	$7.9 \cdot 10^5$

The absolute γ-ray detection efficiency of the CB, including the Si detector and six PPACs inside the sphere, was determined from well-known cascades between 344 keV and 2.75 MeV. Two efficiency conditions were considered: (i) **Sum energy mode**, where energies of all triggered modules are added to recover the total γ energy, yielding efficiencies of 68% at 1 MeV and 55% at 2.75 MeV; (ii) **Neighbour-add mode**, in which energies of adjacent modules are summed if triggered simultaneously, improving the peak-to-total ratio and giving a full-energy efficiency of 62% at 1 MeV.

The Si detector calibration accounted for energy loss in the target and absorbers. Proton calibration was performed using discrete lines from ^{16}O(d,p)^{17}O and ^{12}C(d,p)^{13}C reactions, covering the full relevant energy range.

2.2 Data analysis

The recorded events are categorized into two primary datasets according to trigger type. The first dataset includes signals from the Si ring detector and the Crystal Ball spectrometer, and is used to investigate the γ-decay of the shape isomer ^{236m}U. The second dataset includes events with fission fragments detected by the PPACs in coincidence with the Si ring and CB detectors, and is used to study the delayed fission branch of the isomer.

After calibration, the following observables from the Si detector, PPACs, and Crystal Ball spectrometer are available for analysis:

- E_{Part}: Energy of the light charged particle (proton, deuteron, triton) detected in the Si ring detector.
- t_{Part}: Time of particle detection relative to the accelerator reference signal.

- t_{PPAC}: Time of fission fragment detection relative to the light particle detection.
- $\theta_{\mathrm{PPAC}}, \phi_{\mathrm{PPAC}}$: Emission angles of the fission fragment.
- N_{prompt}: Number of promptly responding NaI modules in neighbour-add (na) mode.
- N_{del}: Number of delayed NaI modules (na mode) within a coincidence time window of 10 ns.
- $\theta_{\mathrm{NaI}}, \phi_{\mathrm{NaI}}$: Angles of the detected γ ray or neutron, used to infer emission direction.
- E_γ: Energy of the detected γ ray.
- E_γ^{Sum}: Total energy (sum) of all detected γ rays.

Analysis of the summed γ-ray energy, E_γ^{Sum}, enables discrimination between prompt and delayed emission. Prompt energy is associated with the initial population of an isomeric state, while delayed energy arises from isomer de-excitation. The high time resolution of the NaI array allows this distinction using a 10 ns coincidence window for delayed γ transitions.

Furthermore, the anode timing from the PPACs permits separation of prompt and delayed fission events. In prompt fission events, such as those following the ^{235}U(d,pf) reaction, the CB spectrometer registers γ-ray cascades from excited fragments and delayed components primarily due to neutron emission. For rare delayed fission events of ^{236m}U, CB data include: (i) γ rays emitted during the isomeric state's population, (ii) delayed γ rays from fission fragments, and (iii) additional energy from delayed neutrons.

The excitation energy E^x of the compound nucleus in (d,p) reactions is determined via the proton energy E_{Prot} deposited in the Si detector:

$$E^x = E_d + Q - E_{\mathrm{Prot}} - E_{\mathrm{Rec}}, \tag{1}$$

where E_d is the deuteron beam energy, Q is the reaction Q-value, and E_{Rec} is the recoil energy. For the ^{235}U(d,p)^{236m}U reaction, this equation provides a direct measure of E^x. In other reactions, such as (d,t) or (d,pn), E^x is appropriately corrected for Q-value differences and particle energy losses in the target and absorbers. For neutron-emitting reactions like (d,pn), the onset of neutron emission defines a threshold in E^x.

A key correlation is established between the excitation energy E^x and the de-excitation energy E_γ^{Sum} recorded by the CB spectrometer. For prompt de-excitations, the energy balance condition is expected:

$$E^x = E_\gamma^{\mathrm{Sum}}. \tag{2}$$

Deviations from this relation are quantified via the missing energy:

$$E_{\mathrm{Miss}} = E^x - E_\gamma^{\mathrm{Sum}}. \tag{3}$$

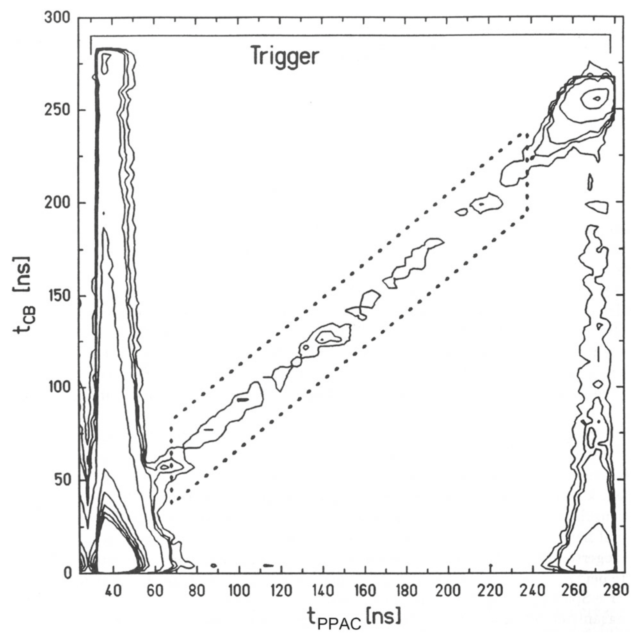

Fig. 3 The PPAC anode time signals t_{PPAC} are plotted against the first delayed NaI time signal t_{CB} of the CB spectrometer for type 4 events. The delayed trigger window is indicated. Delayed fission signals cause the correlated time signals from PPAC and CB detectors in the marked diagonal region. The events that occur within the diagonal time range are caused by delayed fission decay of the shape isomer ^{236m}U

Isomeric states with lifetimes from a few to several hundred ns appear as peaks in the E_{Miss} spectrum at $E_{\mathrm{Miss}} = E_{\mathrm{Iso}}$. The resolution is influenced by undetected prompt transitions and internal conversion processes, leading to asymmetric line shapes. If the isomer decays within the NaI time window, the delayed γ energy $E_{\mathrm{del}}^{\mathrm{Sum}}$ appears as a discrete signal:

$$E_{\mathrm{Miss}} = E_{\mathrm{del}}^{\mathrm{Sum}}. \tag{4}$$

For decays via alternative channels such as fission, the delayed energy is no longer detectable, but the E_{Miss} spectrum still provides access to the excitation energy of the isomer.

A clear identification of the γ-decay of ^{236m}U is achieved through the observation of both delayed γ rays and fission fragments corresponding to its decay branches. Agreement in half-lives of these decay paths, along with consistency in spectra of E^x, E_{Miss}, E_γ^{Sum}, and individual γ lines, confirm the isomer's identity and decay characteristics.

3 Observation of the fission isomer in ^{236m}U

The combined application of the Crystal Ball spectrometer, the parallel-plate avalanche counter (PPAC) system, and the Si ring detector has enabled one of the most detailed inves-

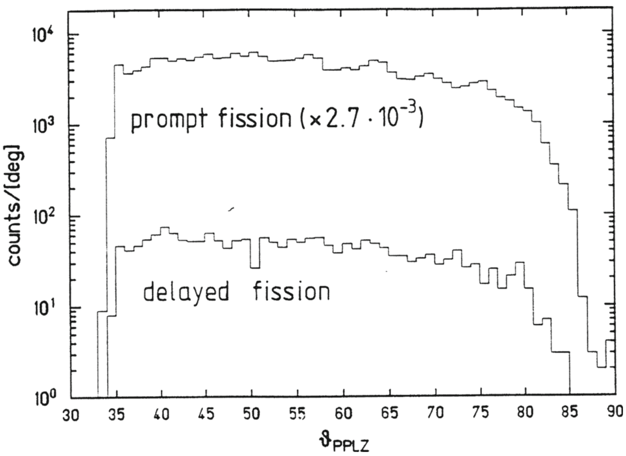

Fig. 4 Angular distribution θ_{PPAC} of fission fragments for prompt and delayed fission events across different cathode combinations. Efficiency losses above $\theta > 80°$ result from increased energy loss in the target

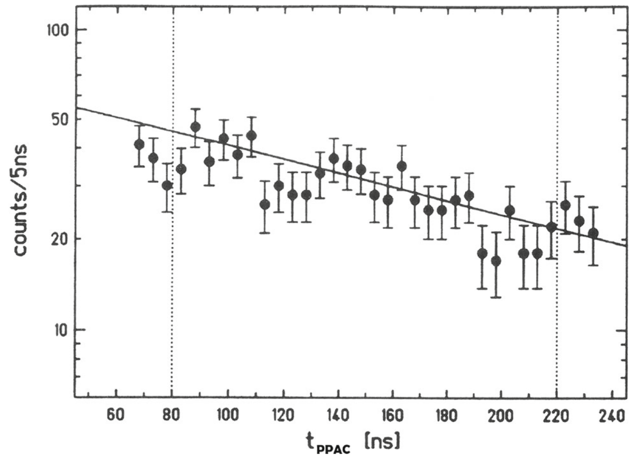

Fig. 5 Time spectrum of delayed fission events relative to the prompt beam pulse. An exponential fit yields a half-life $t_{1/2} = 131 \pm 31$ ns. The fit range is marked by vertical lines

tigations to date of delayed fission from the shape isomer in ^{236m}U. The experimental setup detects all relevant reaction products, excluding conversion electrons. This section demonstrates the successful registration of delayed fission events by the PPAC system. By contrasting these with prompt fission signatures, we validate the capability of the detection method (utilizing the gas counters and the CB) to observe the rare decay channel of delayed fission. The results are in excellent agreement with prior studies on delayed fission in this system, particularly in reproducing the excitation function. This provides a robust foundation for extracting prompt observables that were previously inaccessible and comparing them with independently measured quantities from the γ back decay.

In the data set associated with event type 4, the requirement for detecting a light particle in coincidence with a fission fragment ensures that events originate from the ^{235}U(d,pf) reaction. Though ^{235}U(d,tf) reactions are possible, their significantly lower cross sections at $E_d = 11$ MeV render them negligible as background in the delayed fission channel. Notably, extensive searches for fission isomers in ^{234}U have thus far yielded no positive results.

The delayed fission events are revealed in a plot of the PPAC anode time versus the time of the first delayed NaI signal following the prompt window, attributed to γ rays emitted from excited fission fragments. The selection criteria required at least one NaI detector and one PPAC to deliver prompt time signals. Delayed events (event type 4) populate the t_{PPAC}–t_{CB} plane as shown in Fig. 3. The interval $t_{\text{PPAC}} =$ 28–278 ns defines the hardware trigger window for delayed fission. A low-t_{CB} band within $t_{\text{PPAC}} = 28$–53 ns originates from slowly moving prompt fission fragments that fall within the delayed gate. At $t_{\text{CB}} > 270$ ns, a secondary rise in counts is observed, attributable to subsequent beam pulses. A further population appears at $t_{\text{PPAC}} > 253$ ns with $t_{\text{CB}} < 225$ ns, representing events triggered by the next beam pulse, yet falsely appearing as delayed coincidences.

The genuine delayed fission events from the decay of the ^{236m}U isomer form a distinct diagonal band in Fig. 3. The clear correlation between the delayed fragment and associated γ rays, as well as the response of a prompt NaI detector, forms the basis for further analysis. Events are selected within $\Delta t_{\text{PPAC}} = 68$–$238$ ns and a 45 ns window for delayed NaI signals. The broad time distribution arises from the extended target and variations in energy loss of the fission fragments. Asymmetric mass splits, studied in [23–25], exhibit maxima at $A = 96$ and $A = 140$ with respective kinetic energies of approximately 105 MeV and 75 MeV.

Fragment detection efficiency is affected primarily by their kinetic energy and corresponding energy loss in the target and PPAC materials. Variations due to the emission angles (θ, ϕ) and entrance foil thicknesses have a minor influence on the time-of-flight measurement. The two-dimensional selection shown in Fig. 3 cleanly separates delayed from prompt fission events. Therefore, no further corrections were applied to the anode timing spectrum, particularly as only one fragment per event was detected.

To verify the delayed fission signal, identical angular and position reconstruction techniques were applied to both prompt and delayed events. Figure 4 displays the combined θ_{PPAC} spectra, confirming uniform coverage in the range 35°–80°. The fall-off above 80° stems from the increasing effective target thickness.

Efficiency losses due to fragment stopping in the target were estimated based on the known mass, charge, and energy distributions from neutron-induced fission of ^{236m}U [23–25]. A correction factor of $\epsilon_{\text{target}} = 84\%$ was applied for solid angle losses. The extracted half-life from the anode time

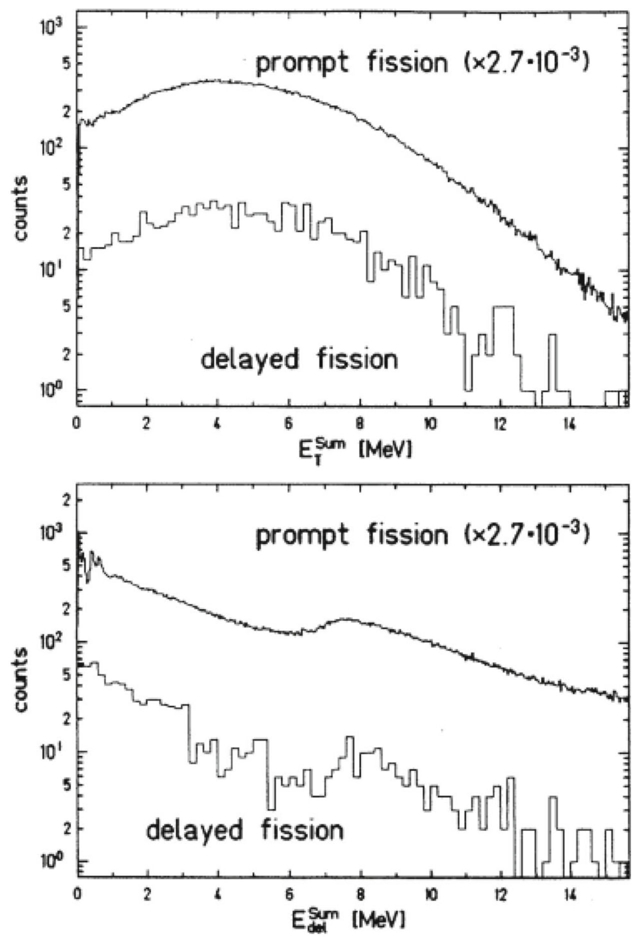

Fig. 6 The upper panel shows the prompt sum energy spectra of the CB (E_γ^{Sum}) recorded for prompt fission events and delayed fission events. For the delayed fission events the prompt time window was adapted to the delayed fission time recorded by the fast PPAC anode signal. The lower panel depicts the delayed sum energy of the CB ($E_{\mathrm{del}}^{\mathrm{Sum}}$) for prompt and delayed fission events. Also in this case the delayed time window is shifted by the delayed fission time. Both spectra feature the characteristic neutron edge at ~ 7.5 MeV caused by neutron capture in NaI and consecutive γ-ray emission (see text for details)

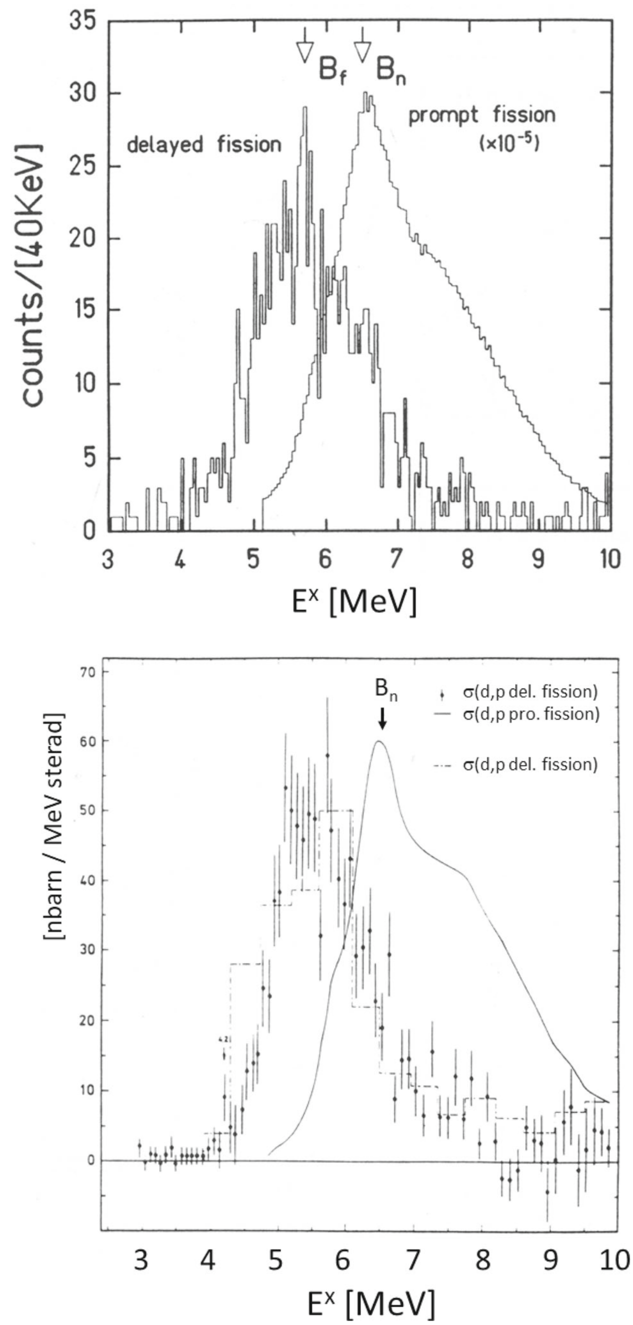

Fig. 7 Excitation energy spectra for prompt and delayed fission events. The delayed fission yields appear below the fission barrier, providing evidence for the population of a shape isomer. The upper panel shows results from the present measurement, while the lower panel reproduces data from Goerlach et al. [28,29]. The previous experiment determined the double differential cross section, $d^2\sigma/d\Omega_p\, dE_p$, for the ^{235}U(d,pf) reaction at an incident deuteron energy of 11 MeV. For comparison, an additional excitation function from Ref. [15] is shown as a dash-dotted line

spectrum is $t_{1/2} = 131(31)$ ns (Fig. 5), consistent with a second fit from the delayed NaI time spectrum: $t_{1/2} = 123(30)$ ns. Both values are in agreement with previous measurements: $t_{1/2} = 110(50)$ ns [26], 105(20) ns [14], 130(15) ns [27], 130(40) ns [15], 116(7) ns [16], 120(15) ns [19], 115(5) ns [21], 137(18) ns [28], and 125(30) ns [1].

NaI signals coincident with delayed fission consist of three components: prompt γ rays emitted during the isomer formation, delayed γ rays from excited fission fragments, and neutron-induced signals following fission. Figure 6 shows that the $E_{\mathrm{del}}^{\mathrm{Sum}}$ spectra exhibit a characteristic enhancement above 6 MeV due to neutron capture, while E_γ^{Sum} from prompt fission declines rapidly in this range. Equivalent spectra are seen for delayed fission, though with a lower overall intensity ($\sim 10^{-5}$). The similarity in spectral shapes indicates the same decay mechanisms following fission, with the time-gated difference in $E_{\mathrm{del}}^{\mathrm{Sum}}$ attributable to the narrower detection window.

Figure 7 illustrates that delayed fission occurs at lower excitation energies ($E^x = 4.3$–6.8 MeV) than prompt fission ($E^x = 5.8$–6.3 MeV). The maximum for delayed fission lies at $E^x = 4.5$–5.3 MeV, below the fission barrier, supporting the hypothesis of a second minimum in the potential energy surface. The observed excitation function closely reproduces the one of Goerlach et al. [28,29], measured under nearly identical conditions, reinforcing the identification of delayed fission from ^{236m}U.

Further evidence for the isomeric decay includes the distinct low-energy structure of the prompt γ spectrum associated with the second minimum. Whereas prompt fission shows a broad, flat maximum at 5 MeV, the isomer's decay features a pronounced peak at $E_\gamma^{\mathrm{Sum}} \approx 1.5$–$1.7$ MeV and no events above 3.5 MeV. At $E^x > B_n = 6.53$ MeV, neutron emission competes with fission, reducing the isomer population probability. Prompt γ multiplicities also differ, with prompt fission yielding a broader distribution (up to six detectors, mean value 7.6), compared to 1–4 γ rays from the isomer region.

The missing energy E_{Miss}, defined as the energy not accounted for by prompt signals in Equation 3, provides a conclusive signature for isomer population. While prompt fission shows a structureless E_{Miss} spectrum, the delayed fission events reveal a peak at $E_{\mathrm{Miss}} = 2.9$ MeV, corresponding to the isomer excitation energy (Fig. 14).

In summary, the following observables confirm the detection of the shape isomer ^{236m}U: (i) delayed PPAC–NaI timing correlations; (ii) prompt and delayed sum energy spectra; (iii) the measured half-life of delayed fission; (iv) the excitation function consistent with previous results; and (v) the observation of missing energy corresponding to the isomeric state. These findings provide compelling evidence for the delayed fission decay of ^{236m}U.

4 Isomeric γ decays following the ^{235}U(d,p) reaction

Figure 8a presents a two-dimensional distribution of excitation energy E^x, calculated for the ^{235}U(d,p)^{236}U reaction, plotted against the prompt total γ-ray energy E_γ^{Sum}. The dominant features correspond to deuteron-induced reactions where the residual nuclei de-excite promptly via γ-ray emission. Events included in this analysis are required to be registered in the Crystal Ball (CB) detector system without any signal in the parallel-plate avalanche counters (PPACs), ensuring a clean selection of prompt γ emissions correlated with charged-particle detection.

Several reaction channels can be identified in the E^x–E_γ^{Sum} plane, demarcated by lines in Fig. 8a–c, based on their characteristic Q values. Line (1), observed at $E^x = 4.65$ MeV, corresponds to elastically scattered deuterons. Due to the high cross section of elastic scattering, this region contains numerous uncorrelated γ-ray signals arising from random coincidences in the NaI detectors, manifesting as a horizontal band.

The ^{235}U(d,p) reaction is represented by the diagonal line (2), where the excitation energy of the residual nucleus corresponds to the sum of γ-ray energies for decays to the ground state. This reaction populates states in ^{236}U up to $E^x \approx 6$ MeV. A decline in intensity beyond this energy is attributed to the onset of competing reaction channels, such as ^{235}U(d,pn) and ^{235}U(d,pf).

A secondary diagonal structure, line (4), arises from the ^{238}U(d,p)^{239}U reaction, due to the presence of approximately 6% ^{238}U in the target material. The lower Q value of 2.57 MeV for this reaction, compared to 4.32 MeV for ^{235}U(d,p), results in a horizontal offset of about 1.75 MeV in the excitation energy. Additional reaction channels identifiable in the 4.5–7 MeV region include: ^{235}U(d,t)^{234}U (line (5)), inelastic scattering ^{235}U(d,d' γ) (line (6)), and ^{238}U(d,t)^{237}U (line (7)). Reactions involving light target impurities are also evident: ^{16}O(d,p)^{17}O (line (8)) and ^{12}C(d,p)^{13}C (line (9)), appearing in the $E^x = 8$–9 MeV range. Known states in ^{17}O and ^{13}C serve as calibration references for the silicon ring detector.

At excitation energies above 6.8 MeV, contour lines emerge due to neutron-emitting reactions such as (d,pn) and (d,pf). Because the neutron energy is not captured in E_γ^{Sum}, the γ-ray sum energy no longer aligns with a diagonal correlation, resulting in a broader distribution. Line (10) reflects the neutron separation energy $S_n = 6.53$ MeV.

Figure 8b applies an enhanced analysis condition, requiring delayed signals in one to three NaI detectors within a 40 ns window following the prompt γ event. A new structure (line (3)) becomes visible, corresponding to the delayed γ decay of the well-known $K^\pi = 4^-$ isomer in ^{236}U at $E^x = 1053$ keV, which decays with a half-life of $t_{1/2} = 101(6)$ ns. The delayed analysis also enhances the contribution of ^{235}U(d,pn) and ^{235}U(d,pf) reactions due to their neutron emission signatures, which are detectable by the NaI array.

A further refinement, shown in Fig. 8c, restricts the delayed detection to one or two responding NaI detectors in a broader 40–260 ns time window. This timing condition suppresses prompt neutron signals, favoring detection of isomeric γ decays. The isomeric cascade in ^{236}U, generally limited to one or two γ transitions, is thus selectively enhanced. Events from the 4^- K-isomer decay continue to appear along line (3) under this condition.

4.1 4⁻ K-isomer in ^{236}U

The 4^- K-isomer in ^{236}U at an excitation energy of $E^x = 1053$ keV exhibits a half-life of $t_{1/2} = 101(6)$ ns. This well-established isomeric decay was used to validate the performance of the Crystal Ball spectrometer for detecting delayed

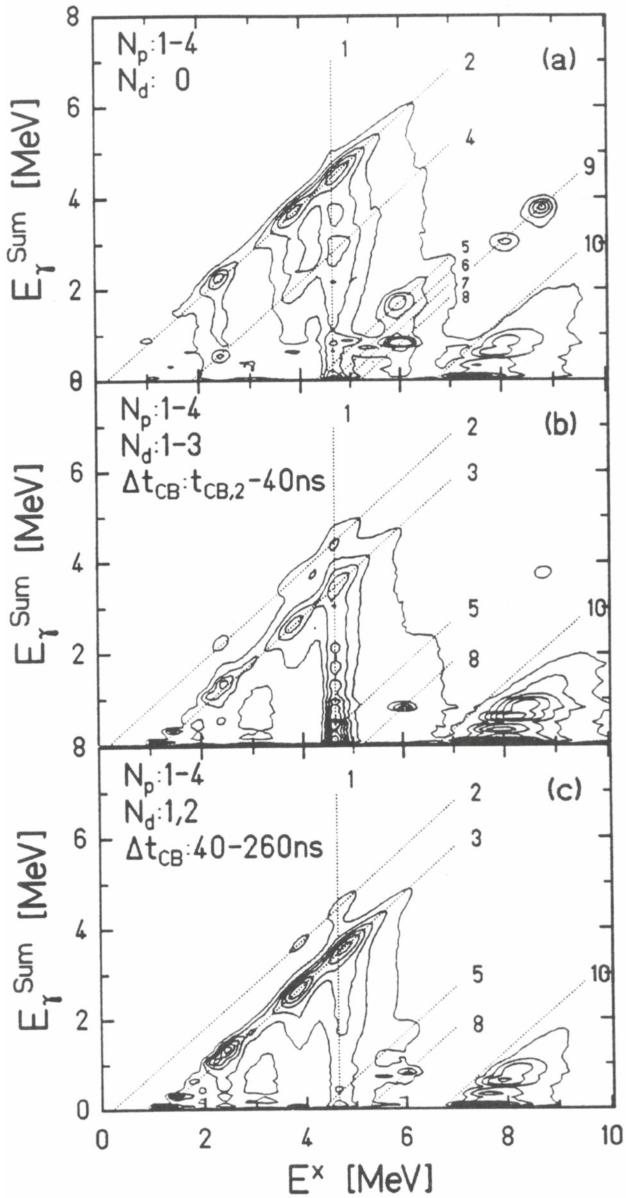

Fig. 8 Excitation energy E^x, calculated for the ^{235}U(d,p) reaction, plotted against the prompt total γ-ray energy E_γ^{Sum} for three distinct analysis conditions. Events include hits in the Crystal Ball detector, with the additional requirement that no signal is recorded in the PPACs. Numbered lines indicate different reaction channels, as described in the text

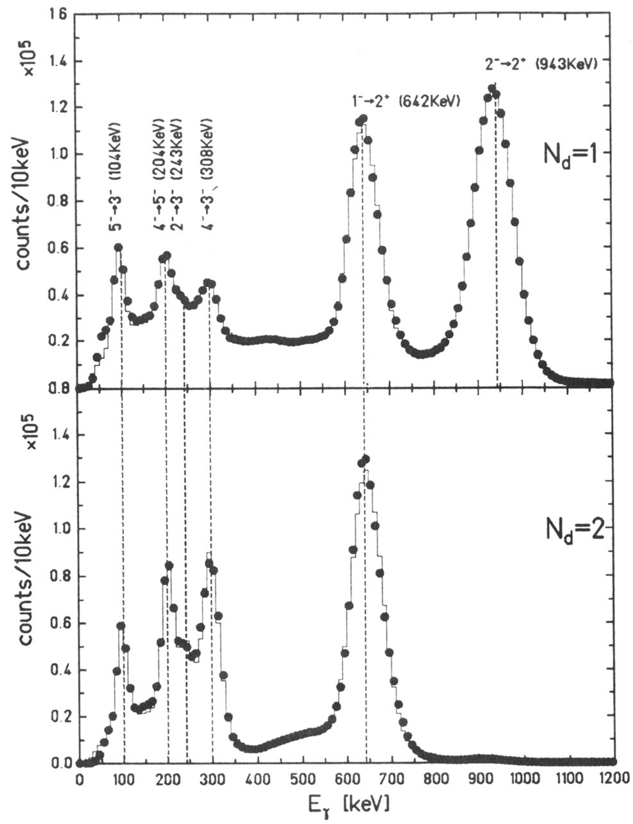

Fig. 9 Measured delayed γ-ray energy spectra associated with the decay of the 4^- K-isomer in ^{236}U at $E^x = 1053$ keV, for events with one (top) and two (bottom) delayed hits ($N_{\mathrm{del}} = 1, 2$) in the Crystal Ball spectrometer

γ-ray emissions. The decay scheme, adopted from Ref. [17], involves at most two observable delayed γ transitions. Several low-energy transitions in the range $E_\gamma = 45$–86 keV are strongly attenuated in γ-ray detection due to high internal conversion coefficients ($\alpha = 597$–105).

Three categories of γ rays can be distinguished based on their energies. First, a direct $E1$ transition connects the isomer to the 4^+ member of the ground-state rotational band. Additional transitions involve negative-parity states at $E^x = 967$ keV (1^-) and 988 keV (2^-), which subsequently decay to the ground state or to the first 2^+ level, emitting γ rays with energies exceeding 900 keV. These transitions differ by only $\sim$20 keV and cannot be resolved individually with the energy resolution of NaI detectors.

Figure 9a shows the delayed energy spectrum for events with $N_{\mathrm{del}} = 1$, recorded in the time window $\Delta t_{\mathrm{CB}} = 40$–280 ns, under the condition that no PPAC signal is present and the prompt energy balance indicates missing energy in the range E_{Miss} =900-1250 keV. This selection effectively isolates isomeric decay cascades. Despite the expectation of single high-energy transitions, additional lower-energy γ rays are observed. These are attributed to partial cascades in which only one transition is detected, or to transitions with significant electron conversion. For example, when the 988 keV state decays to the 688 keV state, the large internal conversion component enhances the observed intensity of the $E_\gamma = 642$ keV transition.

Figure 9b presents the delayed spectrum for events with $N_{\mathrm{del}} = 2$, further constrained by a delayed summed γ energy $E_{\mathrm{del}}^{\mathrm{Sum}} = 650$–1200 keV. A weak peak near 900 keV corresponds to the $4^- \to 4^+$ transition, followed by either a low-energy rotational transition ($4^+ \rightarrow 2^+$ with $E_\gamma = 104$ keV) or a coincident K-shell X-ray. Other observed transitions in Fig. 9a and b originate from the decay of the isomer via negative-parity states of the octupole band, which has a bandhead at $E^x = 688$ keV. The direct decays into the ground-state band from these states produce unresolved γ rays at $E_\gamma = 688$ and 642 keV. Additional transitions in the 200–300 keV range reflect the population and decay of intermediate levels in the octupole band.

The observed γ-ray spectra and decay characteristics of the 4^- K-isomer in ^{236}U are in agreement with established literature values [17], confirming both the known decay scheme and the sensitivity of the CB spectrometer for identifying isomeric transitions.

4.2 γ decay of the shape isomer ^{236m}U

The high detection efficiency of the Crystal Ball spectrometer enables two independent observables for the identification of long-lived isomeric states: (i) the detection of delayed γ decays and (ii) missing energy in the prompt energy balance. Figure 10 presents a two-dimensional correlation plot of the missing energy E_{Miss} versus the delayed total energy $E^{\mathrm{Sum}}_{\mathrm{del}}$, based on events fulfilling the following criteria: (i) two delayed NaI detectors trigger in coincidence within $\Delta t = 10$ ns, (ii) the number of prompt NaI detector hits is $N_{\mathrm{prompt}} = 1$–4, (iii) delayed NaI signals are recorded in the time window $\Delta t_{\mathrm{CB}} = 40$–200 ns, (iv) no delayed signals are present in the 0–40 ns interval or after $t_{\mathrm{CB}} > 200$ ns, thereby excluding contributions from subsequent beam pulses, (v) the excitation energy lies within $E^x = 4.3$–6.8 MeV, and (vi) no signal is recorded in the PPAC.

The condition $E_{\mathrm{Miss}} = E^{\mathrm{Sum}}_{\mathrm{del}}$ selects candidate events for isomeric γ decays. A pronounced peak is observed at 1053 keV, corresponding to the known 4^- K-isomer. The broader distribution toward higher E_{Miss} is attributed to incomplete detection of prompt γ rays feeding the isomer, primarily due to internal conversion and detector inefficiencies.

A second distinct peak appears at $E_{\mathrm{Miss}} = 2.8$ MeV and is attributed to the decay of the shape isomer in ^{236m}U, previously observed in Ref. [1]. This feature is consistently present in the projections of both E_{Miss} and $E^{\mathrm{Sum}}_{\mathrm{del}}$. A separate, energy-shifted diagonal region is used for background estimation; its projections (dash-dotted) help exclude contributions not associated with isomeric decays.

A peak at $E_{\mathrm{Miss}} = 1.75$ MeV does not have a corresponding structure in the $E^{\mathrm{Sum}}_{\mathrm{del}}$ projection and is thus not assigned to an isomeric decay. The broad band of events in this region is interpreted as background, likely stemming from β decays of nuclei such as ^{28}Al, which may form via the ^{27}Al(d,p) reaction or neutron capture in aluminum structures. The β decay of ^{28}Al populates the 1778 keV state in ^{28}Si, which

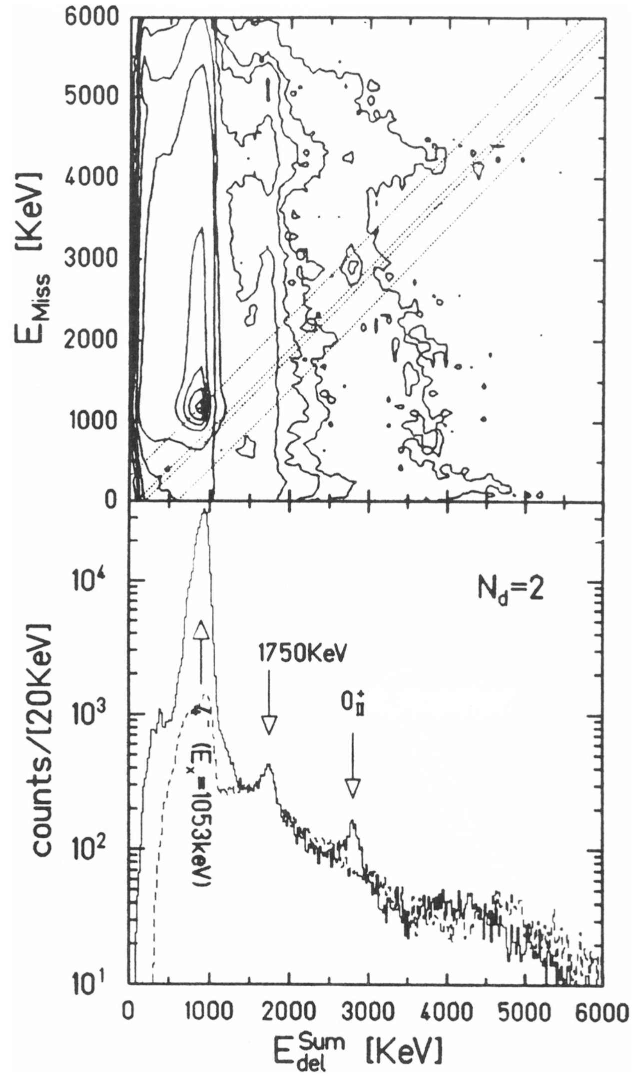

Fig. 10 Two-dimensional plot of missing prompt energy E_{Miss} versus delayed summed energy $E^{\mathrm{Sum}}_{\mathrm{del}}$. Isomeric decays are observed along the diagonal region, where energy conservation is satisfied. The projections of the diagonal band reveal peaks corresponding to the known 4^- K-isomer and the shape isomer in ^{236}U at $E_\gamma = 1053$ keV and 2800 keV, respectively. A shifted diagonal region is used to estimate background contributions (dash-dotted lines). Notably, a peak at 1750 keV in E_{Miss} is absent in the $E^{\mathrm{Sum}}_{\mathrm{del}}$ projection and is thus not attributed to an isomeric decay

subsequently emits a γ ray. Given the 2.24-min half-life of ^{28}Al, these decays are uncorrelated in time with beam pulses and appear as non-isomeric background.

Additionally, a broad structure above $E_{\mathrm{Miss}} > 3.8$ MeV is seen in both isomeric and background spectra, without a corresponding peak in $E^{\mathrm{Sum}}_{\mathrm{del}}$. These events are likely due to (d,d'), (d,d'γ), or (d,t) reactions on ^{235}U, consistent with observations in Sect. 4.

To explore the multiplicity dependence of the isomeric decay signal, the analysis was extended to events with one or three delayed detector hits. Figure 11 presents the projections

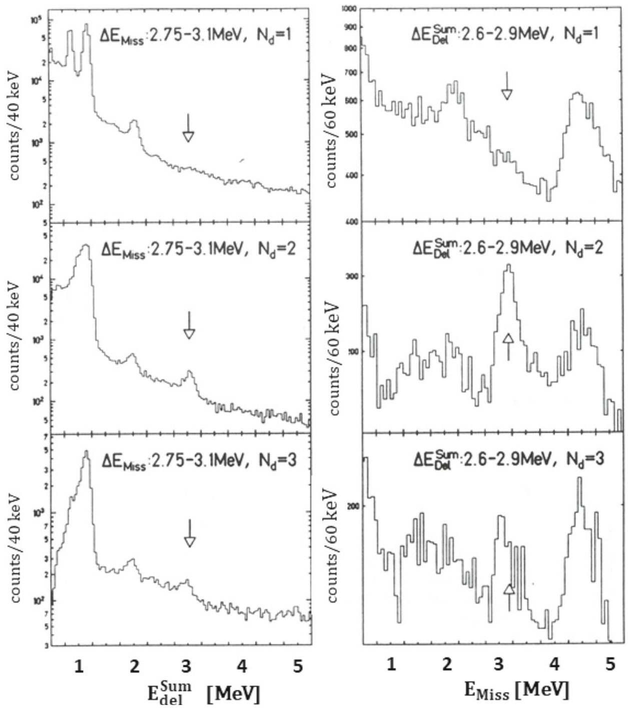

Fig. 11 Projections of the $E_{\mathrm{del}}^{\mathrm{Sum}}$–$E_{\mathrm{Miss}}$ plane for delayed NaI multiplicities $N_{\mathrm{del}} = 1$, 2, and 3 onto both energy axes. A direct transition with $N_{\mathrm{del}} = 1$ from the second potential minimum is not observed

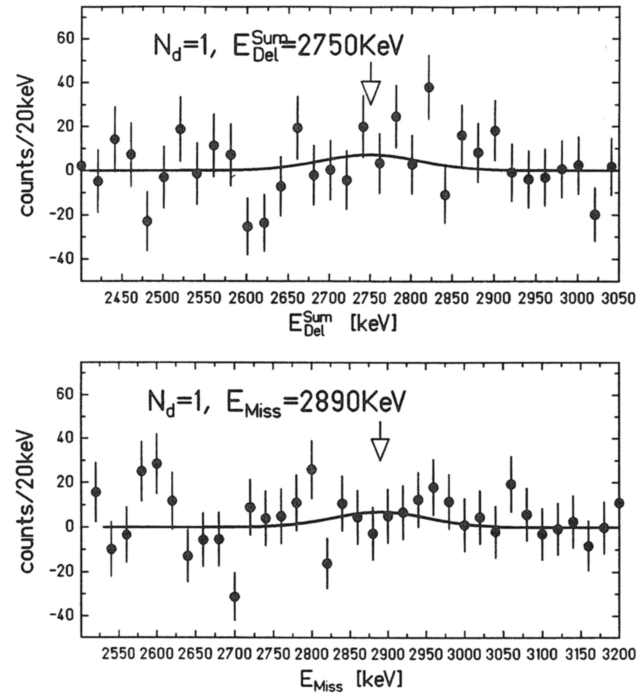

Fig. 12 Search for a possible direct single-step γ decay from the shape isomer to the 2^+ state in the first minimum. (**a**) $E_{\mathrm{del}}^{\mathrm{Sum}}$ spectrum for $N_{\mathrm{del}} = 1$, centered at 2750 keV. (**b**) Corresponding E_{Miss} spectrum, based on an assumed excitation energy of $E^x = 2814$ keV. No statistically significant signal is observed in either spectrum, and only upper limits are derived

for $N_{\mathrm{del}} = 1, 2$, and 3. The isomer signal is most prominent for $N_{\mathrm{del}} = 2$, while for $N_{\mathrm{del}} = 3$ it appears with reduced intensity. No significant peak is observed for $N_{\mathrm{del}} = 1$, suggesting that a direct one-step γ decay from the highly deformed second minimum to the first minimum is strongly suppressed.

The possibility of a direct γ transition from the isomeric state to the 2^+ state in the first potential minimum, with $E^x = 45$ keV, is further examined. Figure 12a presents the $E_{\mathrm{del}}^{\mathrm{Sum}}$ spectrum for events with $N_{\mathrm{del}} = 1$, in the range $E_{\mathrm{del}}^{\mathrm{Sum}} = 2400$–$3050$ keV. The marked energy $E_{\mathrm{del}}^{\mathrm{Sum}} = 2750$ keV corresponds to the transition energy difference, as inferred from cascades observed in events with $N_{\mathrm{del}} = 2$ and 3. The corresponding E_{Miss} spectrum is shown in Fig. 12b. Backgrounds are fitted with parabolic functions using two full-width intervals on either side of the signal region. Line widths were set according to the measured resolution.

A χ^2 fit to the spectra yields integrated peak areas of 69 ± 61 counts in the $E_{\mathrm{del}}^{\mathrm{Sum}}$ spectrum and 55 ± 64 counts in the E_{Miss} spectrum, both consistent with zero within statistical uncertainties. Consequently, no statistically significant evidence is found for a direct one-step γ transition from the isomer, and only upper limits can be established for this decay pathway.

5 Common properties of the fission isomer ^{236m}U and the γ decay of the 2.8 MeV isomer

The γ-decay of the shape isomer in $^{236\mathrm{m}}$U was previously reported by Schirmer et al. [1], with the identification based on comparisons to earlier measurements of the fission isomer. The extracted half-life and excitation function agreed with earlier data from delayed fission studies, such as those reported by Goerlach et al. [28,29]. The extended experimental configuration used in the present work allows, for the first time, simultaneous observation of both decay modes – γ decay and delayed fission – originating from the same isomeric state. This enables a comprehensive comparison encompassing not only the half-lives and excitation functions, but also the missing prompt energy and the prompt γ-ray cascades feeding the second potential minimum (II. minimum).

The half-life extracted from the γ-decay channel, $t_{1/2} = 119 \pm 15$ ns, is in good agreement with values obtained from the delayed fission channel, $t_{1/2} = 123 \pm 30$ ns (from delayed NaI timing) and $t_{1/2} = 131 \pm 31$ ns (from PPAC timing). These values are consistent within uncertainties with earlier measurements, including $t_{1/2} = 124 \pm 40$ ns from Ref. [1] and the weighted average of $t_{1/2} = 123 \pm 19$ ns derived from earlier delayed fission experiments.

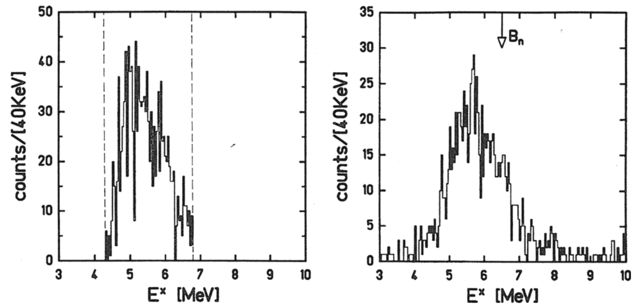

Fig. 13 Excitation energy spectra E^x for γ decay (left) and delayed fission (right). Both decay modes exhibit similar population patterns of the isomeric state

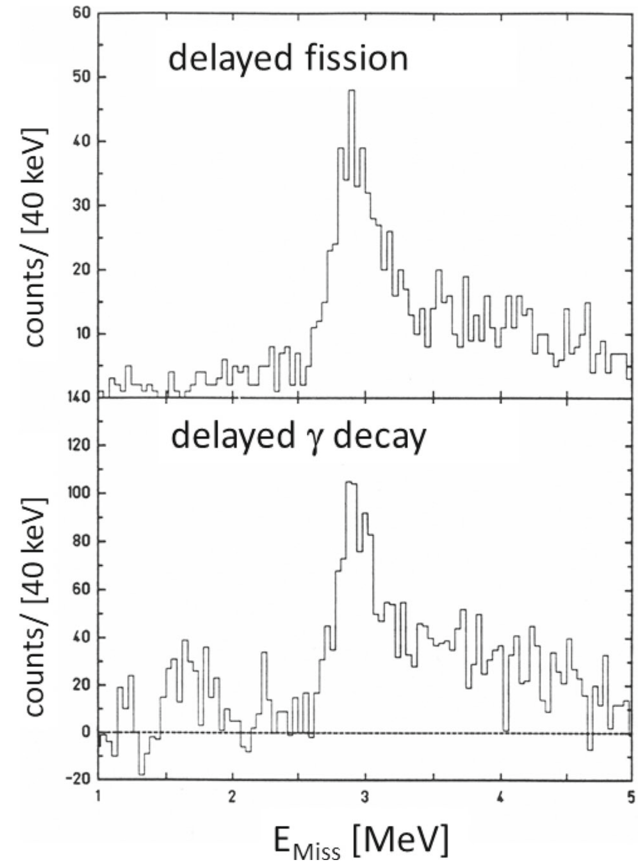

Fig. 14 Comparison of missing prompt energy E_{Miss} for delayed fission and γ decay. Both spectra show a consistent peak at ∼2.9 MeV, indicating a shared isomeric origin

As shown in Fig. 13, the excitation energy spectra E^x for both decay modes are in excellent agreement within statistical uncertainties. A cut on excitation energy (4.3 MeV $\leq E^x \leq$ 6.8 MeV) was applied to the γ-decay events to enhance signal purity. This window encompasses 85% of delayed fission events, ensuring that the selected γ decays are representative of the same excitation region without introducing significant efficiency losses.

A crucial cross-check is provided by the spectrum of the missing prompt energy E_{Miss}, which reflects undetected components of the prompt cascade feeding the isomeric state. Figure 14 compares E_{Miss} spectra for delayed fission (no background subtraction, two-dimensional timing via t_{PPAC} and t_{CB}) and background-subtracted γ decays. Both spectra exhibit a pronounced peak at $E_{\mathrm{Miss}} \approx 2.9$ MeV with negligible contributions below 2.5 MeV. The consistency in peak position and width between the two decay modes supports a common origin from the same isomeric state.

It should be noted that the E_{Miss} spectrum does not directly yield the isomer's excitation energy, which is independently reconstructed from the total delayed γ energy. Shifts toward higher E_{Miss} are primarily due to internal conversion and detection inefficiencies, especially in low-energy rotational transitions. These features, observed in prior spectroscopy studies, account for the higher-energy tail in the E_{Miss} distribution, which remains consistent between the two decay modes.

The presence of a shared isomeric state is further supported by the agreement in prompt γ spectra feeding the isomer. If the decays originated from two distinct isomers at the same excitation energy – e.g., a weakly populated isomer in the normally deformed first minimum – marked differences would arise in the prompt γ-ray spectra. Instead of the collective low-energy transitions characteristic of superdeformation, one would expect complex feeding from the dense level scheme of a normally deformed nucleus. The observed spectral features, however, clearly support a superdeformed character consistent with the known fission isomer.

Prompt γ spectra were analyzed using the neighbour-add method and are categorized by multiplicity $N_p = 2$–4 for both decay channels, as shown in Fig. 15. Contributions at higher multiplicities were negligible. The spectra for γ decay (left panels) were selected using a window along the diagonal in the E_{Miss}–$E_{\mathrm{del}}^{\mathrm{Sum}}$ plane, with an excitation energy cut of $4.3 \leq E^x \leq 6.8$ MeV to ensure proper energy balance.

To ensure correct excitation to the isomeric state at $E =$ 2.8 MeV, events with $E_\gamma^{\mathrm{Sum}} < 1.5$ MeV or > 4.0 MeV were excluded. While the upper threshold had no effect on the spectra, the lower bound removes events with substantial undetected energy. This condition applies only to γ-decay events, explaining the absence of low-energy entries in the $N_p = 1$ spectrum, which peaks between 1.5 and 2.9 MeV. At higher multiplicities ($N_p = 2$–4), the average detected energy is higher, and the impact of this threshold is negligible.

In both decay modes, the prompt spectra for $N_p = 2$ display consistent features, including a dominant peak at $E_\gamma \approx$ 800 keV and a secondary peak between 1200–1300 keV. For $N_p = 3$ and 4, the agreement is even more striking. A prominent line at $E_\gamma \approx 800$ keV and enhanced intensity between 230–350 keV appear in both data sets. Background correc-

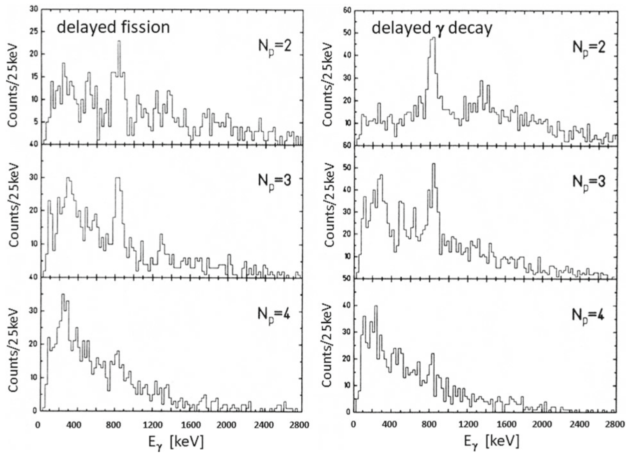

Fig. 15 Prompt γ-ray energy spectra feeding the isomeric state for delayed fission and γ decay. Spectra are sorted by multiplicity $N_p = 2$–4 and show excellent agreement

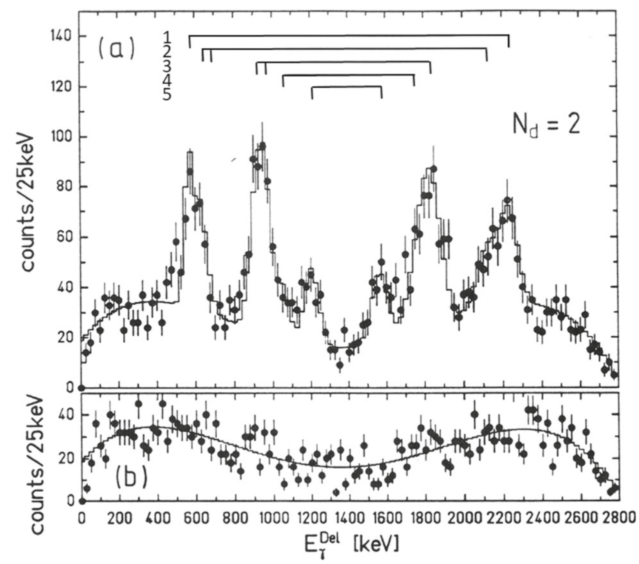

Fig. 16 Single-energy spectrum of delayed γ decay from the shape isomer in ^{236m}U via two γ rays, fitted with five decay cascades. Numbers aside the lines refer to the five cascades of Table 2. Dominant cascades 2 and 3 proceed through known 1^- states in the first minimum. The intensities of the two lines were constrained to agree within statistical and background uncertainties. Peak widths were fixed by the experimental energy resolution. The background (panel **b**) is modelled by a fourth-order polynomial

tions, applied only to the γ-decay spectra, show no significant contributions in these regions.

These findings confirm that the observed γ decays stem from the shape isomer located in the second potential minimum of ^{236}U, which also undergoes delayed fission. The two decay channels correspond to tunneling through the outer barrier (fission) or inner barrier (γ decay to the normally deformed first minimum). The excellent agreement in decay lifetimes, excitation functions, missing energy distributions, and prompt γ spectra provides strong evidence for the identification of a single isomeric state with two competing decay paths. Moreover, the observation of two- and three-step feeding cascades opens the door to detailed γ-spectroscopic studies and level correlations in the superdeformed potential well.

6 Decay cascades

Further investigations focus on decays via two- and three γ rays. Throughout the analysis, the energy ranges $E_{\text{del}}^{\text{Sum}} =$ 2.6–2.9 MeV and $E_{\text{Miss}} =$ 2.75–3.1 MeV define the “isomer window”. Background is extracted from $E_{\text{del}}^{\text{Sum}} = 2.6$–2.9 MeV and $E_{\text{Miss}} = 2.35$–2.7 MeV, directly below the isomer region on the E_{Miss} axis. Background windows at higher E_{Miss} energies are unsuitable, as they may include decay components arising from incomplete detection of prompt γ rays, either due to cascade detection inefficiencies or transitions involving conversion electrons. Both effects, particularly relevant at low γ-ray energies and in highly deformed systems, shift E_{Miss} values higher and will be discussed in detail later.

Alternative background selections – such as windows at the same E_{Miss} but different $E_{\text{del}}^{\text{Sum}}$ values – are also inappropriate, as the steeply falling $E_{\text{del}}^{\text{Sum}}$ spectrum would misrepresent the background. Moreover, symmetric or low-$E_{\text{del}}^{\text{Sum}}$ windows neglect the efficiency losses for delayed γ-ray detection. The adequacy of the chosen background is demonstrated in Fig. 16b, where the $N_{\text{del}} = 2$ single-energy spectrum shows no peak structures. Its intensity matches that of the isomer window spectrum (Fig. 16a) at low ($E_\gamma < 400$ keV), high ($E_\gamma > 2400$ keV), and intermediate ($E_\gamma \approx 1300$ keV) energies. A fourth-order polynomial fit accurately reproduces the background and is used in the subsequent line fitting.

The single-energy spectrum gated on the isomer window (Fig. 16a) exhibits discrete entries corresponding to two-step cascades, also listed in Table 2. Beyond the background component, Gaussian fits were applied to extract the transition energies. Pairs of transitions were identified such that their summed energy satisfied $E_{\text{del}}^{\text{Sum}} = 2800 \pm 50$ keV. As a result of the fitting, five cascades can be determined, the energy values and intensity distributions of which are given in Table 2. The absolute intensity of the fitting comprises 950 ± 50 decays, with an almost equally large background component. These values are also obtained in a global evaluation of the E_{Miss} or $E_{\text{del}}^{\text{Sum}}$ spectrum with 920 or 970 decays, respectively, from which it is concluded that all decay cascades are found.

In cascade 1, with $E_\gamma = 580$ keV and $E_\gamma = 2239$ keV, the low-energy γ ray must be emitted first; otherwise, the 580 keV transition would require an intermediate state in the first minimum, where no relevant states are known between

Table 2 Energies and intensities of the five decay cascades according to Fig. 16. The energy values in parentheses in lines 2 and 3 correspond to the alternative transition energies that result from the known branching ratios for the γ-decay transitions from the excited states to the ground state and the first excited 2^+ state, unable to be resolved with NaI energy resolution. For further details, see the main text

	$E_{\gamma 1}$ [keV]	$E_{\gamma 2}$ [keV]	Sum [keV]	Intensity
1	580 ± 15	2239 ± 35	2819 ± 38	13.5%
2	2129 ± 25	$686(642) \pm 10$	2815 ± 29	20.3%
3	1842 ± 15	$967(920) \pm 10$	2809 ± 21	38.8%
4	1061 ± 45	1755 ± 50	2816 ± 67	10.3%
5	1214 ± 20	1576 ± 30	2790 ± 36	15.6%

522 and 688 keV [17]. This decay order is supported by (γ, γ') measurements on ^{236}U [30], which identified a state at $E = 2243.9$ keV, consistent within experimental resolution. This state, likely of spin 1, decays predominantly (95.7%) to the ground state. Although no $E1$ or $M1$ assignment was done, the absence of decay to the 2^+ state suggests it is not 1^+. Similar cases, clarified through polarization measurements, favored $E1$ assignments. Thus, cascade 1 likely proceeds via a 1^- state at 2243.9 keV.

In cascades 2 and 3, the low-energy transitions originate from the decay of known 1^- states at $E^x = 688$ keV and $E^x = 967$ keV. These states decay via known branching ratios either to the ground state or to the 2^+ rotational state at 45 keV, which is fully converted. In the fit procedure, the energies and intensity ratios of this unresolved doublet were fixed according to Ref. [17].

To describe the spectrum between 1000 and 1700 keV, two additional cascades, labelled 4 and 5, were fitted. Cascade 4, having the smallest branching ratio, cannot be clearly resolved and may represent a superposition of several states. As with cascade 1, the emission order of the γ rays is uncertain. Cascade 4, with $E_\gamma = 1061 \pm 45$ keV and $E_\gamma = 1755 \pm 50$ keV, can be interpreted either as a decay via an intermediate state at 1807 keV, known from β decay of ^{236}Pa and transfer reactions on ^{235}U, or through a state at 1110 keV, likely a 2^+ state. The expected secondary transitions are 1762 keV (73%) and 1807 keV (23%) in the first case (average 1773 keV), or 1065 keV in the second. The ordering of the transitions in cascade 4 was investigated by considering the possible decay paths of the two intermediate states and the intensities of these decay paths. If the decay path via the state at 1110 keV was correct, approximately 55% of its intensity would be expected in the $N_{\mathrm{del}} = 3$ spectrum. However, no corresponding transitions are observed, despite sufficient sensitivity to detect intensities as low as 30%. Therefore, cascade 4 proceeds via the state at $E_\gamma = 1807$ keV, decaying either directly to the ground state or, indistinguishably, to the 2^+ state at $E_\gamma = 45$ keV. As expected no signal

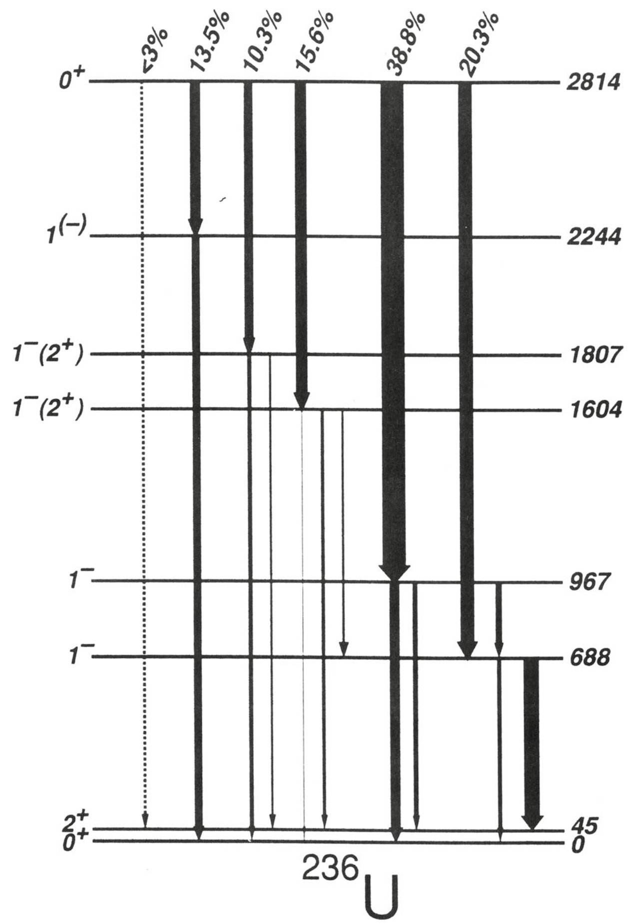

Fig. 17 Decay scheme of the shape isomer at $E^x = 2814 \pm 33$ keV. The relative intensities of the five decay cascades are shown, along with an upper limit for a potential transition to the 45 keV state. For the 1604 keV level, only the most intense transitions are indicated

is observed in the $N_{\mathrm{del}} = 3$ spectrum for this intermediate state.

A similar scenario arises in cascade 5. The intermediate state may correspond either to a level at 1604 keV, previously identified as a 1 or 2^+ state, or to a 1271 keV level known from the β decay of $^{236\mathrm{m}}$Pa, listed in Ref. [17] as a possible (1^-, 2, 3) state. In both cases, the measured transition energies are consistent with dominant decay paths. For the 1604 keV state, γ rays of 1604 keV (6.9%) and 1559 keV (38%) are observed, yielding a measured energy of 1575 keV. In the case of the 1271 keV level, a 1225 keV transition is emitted in 61.5% of decays, matching the observed 1214 keV line. However, the intermediate state cannot be unambiguously identified in the $N_{\mathrm{del}} = 2$ spectrum. Therefore, additional information was extracted from the more selective $N_{\mathrm{del}} = 3$ data.

The individual energy spectrum for three delayed detectors were obtained under the isomer conditions $E^{\mathrm{Sum}}_{\mathrm{del}} = 2.6$–2.9 MeV and $E_{\mathrm{Miss}} = 2.75$–3.1 MeV, along with the corresponding background spectrum. Compared to previous spectra, a more restrictive analysis was applied: events with delayed neighbouring detector responses were excluded (anti-Compton mode), enhancing line shape quality, which is particularly beneficial under the $N_{\text{del}} = 3$ condition. Unlike the $N_{\text{del}} = 2$ case, pronounced peaks appear at $E_\gamma \approx 300$ keV and $E_\gamma = 600$–700 keV. To interpret these and other features, conditions were applied to specific transitions. In the dominant three-step cascade, the state at 967 keV, following high-energy gamma emission, decays either directly to the ground state or, in 30% of cases, via the 688 keV state through a 279 keV transition, similar to cascade 2. This three-step sequence is clearly visible in the spectrum and is confirmed by gating on the involved transitions. Two peaks are observed in each gated spectrum at $E_\gamma \approx 300$ keV, 660 keV, and 1850 keV, while the gating transition itself is suppressed.

Cascade 5 was further investigated using energy spectra gated on transitions populating intermediate levels in three-step cascades. The results support a decay pathway through a 1^- state at 1604 keV, populated via a 1224 keV transition. All expected transitions for this pathway are observed. Conversely, the alternative scenario involving a 1271 keV (2^-) state is strongly disfavored due to the absence of corresponding γ rays in the spectrum gated on the 1530 keV transition.

The excitation energy of the isomer was deduced from three cascades, using the measured transition energies and the known energies of the intermediate states and their literature values. The resulting value is $E^x = 2814 \pm 33$ keV, where the uncertainty includes only contributions from feeding transition energies. This value is consistent with the energy extracted from a fit to the $E_{\text{del}}^{\text{Sum}}$ spectrum, $E^x = 2790 \pm 20$ keV, after accounting for possible energy losses of 45 keV due to transitions to the 2^+ state. The present result is slightly higher than that reported in Ref. [1], which determined $E^x = 2750 \pm 10$ keV.

In summary, the observed back-decay pathways – including the measured transition energies and the established levels in the first potential minimum of ^{236}U – allow for the identification of five cascades accounting for the γ decay intensity. These decays proceed through 1^- or dipole states with likely electric dipole ($E1$) transitions. Compared to the findings in Ref. [1], the present results align well with known states of ^{236}U and can be interpreted without invoking additional intermediate levels. The data provide strong experimental support for the hypothesis that the intermediate states in these cascades are predominantly 1^- states. The proposed decay scheme is summarized in Fig. 17.

7 Branching ratios

The simultaneously measured decay paths of the shape isomer allow a direct determination of the following branching ratios. The branching ratio Γ_γ/Γ_f is directly determined from the measured number of back-decay events, $N_\gamma = 1300 \pm 80$, and delayed fission events, $N_{\text{fis}} = 1137 \pm 34$. These raw counts must be corrected for detection efficiencies, which are composed of several independent components. The detection efficiency for the backscattered proton is not relevant, as it applies equally to both decay channels and therefore cancels out in the branching ratio. The total detection efficiency for delayed decay must account for the following loss factors:

- $\epsilon(E_{\text{del}}^{\text{Sum}}) = 0.33 \pm 0.03$: This factor arises from the analysis condition in the $E_{\text{del}}^{\text{Sum}}$–$E_{\text{Miss}}$ plane, which requires full energy deposition of the delayed γ cascade. Efficiency losses associated with delayed cascades were previously addressed in the calculation of the intensity ratios of the back decay.
- $\epsilon(E_\gamma^{\text{Sum}}) = 0.35 \pm 0.01$: This efficiency reflects the requirement to detect the full sum energy of the prompt cascade. It is derived from the delayed fission data, where this condition is not mandatory but can be applied additionally.
- $\epsilon(E^x) = 0.85 \pm 0.01$: The requirement for the excitation energy to lie between 4.3 and 6.8 MeV leads to a minor efficiency loss of approximately 15%, as directly evident from the excitation function of delayed fission.
- $\epsilon(\Delta t_\gamma) = 0.40 \pm 0.01$: Time-window losses are evaluated using the crystal ball timing calibration. Deviations from the nominal timing are below 1% across all detectors, and corrections are guided by the known half-life of the isomer.

For delayed fission events, the following efficiency components must be taken into account:
- $\epsilon(\text{PPAC}) = 0.60 \pm 0.04$: The efficiency of the parallel plate avalanche counters (PPACs) for fission fragments is estimated to exceed 96%. The remaining loss is predominantly due to uncovered solid angle segments.

- $\epsilon(\text{Target}) = 0.84 \pm 0.02$: The likelihood of a fission fragment being stopped in the target material, or slowed to undetectability, was evaluated in Sect. 3.
- $\epsilon(E_\gamma) = 0.95 \pm 0.01$: For detecting delayed fission, the crystal ball must respond to both prompt and delayed signals. Since only a single energy and time signal is required for each cascade, the high response probability of the NaI detectors – given the observed multiplicity and energy distribution of the transitions – leads to only a minor efficiency correction.

– $\epsilon(\Delta t_f) = 0.45 \pm 0.01$: The time-window efficiency for delayed detection is determined based on the timing response of the system.

The efficiency factors and their associated uncertainties are determined by the decay pathways, the different detectors involved, and the various measured observables. These sources of uncertainty are considered statistically independent. An exception arises in the delayed detection efficiency of the Crystal Ball, which is slightly affected by the preceding prompt cascade: prompt detections occupy some counters, reducing those available for delayed detection. Nevertheless, the generally low prompt and delayed multiplicities, combined with the high granularity of the detector, lead to only minimal distortions in efficiency. This effect is accounted for by assigning a slightly reduced detection efficiency and an increased uncertainty to the delayed detection.

The relative uncertainties for the two decay modes are comparable and contribute to a total uncertainty in the branching ratio of $\Delta = 12.4\%$. Accordingly, the branching ratio is determined to be $\Gamma_\gamma/\Gamma_f = 6.5 \pm 0.8$, in agreement with previous estimates. Reported values in the literature span a broad range, including $\Gamma_\gamma/\Gamma_f < 1.5$ [20], $\Gamma_\gamma/\Gamma_f \approx 10$ [15], $\Gamma_\gamma/\Gamma_f \approx 6$ [21], $\Gamma_\gamma/\Gamma_f = 7 \pm 2$ [31], and $\Gamma_\gamma/\Gamma_f = 8 \pm 3$ [1].

The ratio of prompt fission from the (d,pf) reaction to delayed fission from the shape isomer can be extracted directly from the present measurement. Identical detector setups were used for both prompt and delayed fission channels, involving detection of the backscattered proton and the fission fragment, and both processes were triggered identically. As a result, only minimal corrections are required when evaluating the ratio. Background contributions from (d,d'f) and (d,f) reactions were effectively suppressed through appropriate gating on the proton detector. Furthermore, only events with excitation energies $E^x > 5.1$ MeV were included in the analysis. For delayed fission, the detection efficiencies $\epsilon(E_\gamma)$ and $\epsilon(\Delta t_f)$ were incorporated to account for differences in detection probabilities between prompt and delayed channels.

The ratio of proton-induced delayed to prompt fission is thus $\Delta\sigma(d, pf_{\mathrm{del}})/\Delta\sigma(d, pf) = (4.9 \pm 0.2) \cdot 10^{-5}$ which is comparable to the ratio $(5.9 \pm 1.8) \cdot 10^{-5}$ from a previous measurement [28].

8 Discussion and conclusion

The combined use of the Crystal Ball spectrometer, the parallel-plate avalanche counter (PPAC) system, and charged-particle detector has enabled the most detailed study to date of the fission isomer $^{236\mathrm{m}}$U. All relevant reaction products, except conversion electrons, were detected with high efficiency, allowing the two decay branches – γ back-decay and delayed fission – to be observed independently and with high selectivity.

In the case of the gamma decay branch, the selective population and clean identification of the ^{236}U nucleus via the ^{235}U(d,p)^{236}U reaction were achieved through carefully chosen analysis conditions. Background contributions were effectively suppressed using two powerful analysis tools: (i) the two-dimensional plane of excitation energy E^x versus the prompt total gamma energy E_γ^{Sum}, and (ii) the plane of missing energy E_{Miss} versus the delayed total gamma energy $E_{\mathrm{del}}^{\mathrm{Sum}}$.

The delayed fission branch was confirmed by direct comparison with prompt fission events from the ^{235}U(d,pf) reaction. The detection scheme – based on the coincidence of fission fragment detection in PPACs with γ-ray calorimetry in the Crystal Ball – allowed to identify this exceedingly rare decay mode. The results are consistent with previous measurements of delayed fission from $^{236\mathrm{m}}$U, in particular reproducing the excitation function with high accuracy.

Several observables related to the population and decay of the shape isomer $^{236\mathrm{m}}$U, which were not accessible in earlier experiments, have now been extracted. These were independently compared for both the γ decay and the delayed fission branches. As a result, compelling evidence is provided that both decay paths originate from the same isomeric state:

1. The half-lives of the gamma decay and delayed fission branches are identical within experimental uncertainty.
2. The excitation energy distributions for both decay modes exhibit the same characteristics.
3. The missing prompt energy E_{Miss} is identical and independent of the decay mode.
4. The gamma-ray energy spectra associated with the population of the second potential minimum are consistent for both decay paths.

The γ-decay branch, investigated here with improved statistical accuracy, yielded following results:

1. The excitation energy of the isomeric ground state in the second potential minimum is determined to be 2814 ± 33 keV.
2. The decay proceeds through five distinct cascades via known 1^- states of the normally deformed ^{236}U.
3. A single-step gamma decay of $^{236\mathrm{m}}$U into the first excited 2^+ state at $E^x = 45$ keV is excluded, with an upper limit established.

The comparison with the previous results of Schirmer et al. [1] reveals overall very good agreement and supports the earlier conclusions. The decay of the shape isomer proceeds via an intermediate state in normally deformed ^{236}U.

The improved statistics and new spectroscopic data on ^{236}U enable the identification of all intermediate states involved in the decay path. These states correspond to known low-spin levels, and are, with some probability, also 1^- states. The strongest decay branches proceed through the first and second 1^- states, consistent across both the present and earlier experiments.

With respect to the excitation energy, the new data yield a value of 2814 ± 33 keV, which is 60 keV higher than the value reported by [1]. This excitation energy was determined in a similar manner, by fitting transition energies using peaks of known width.

The $B(E1)$ transition probabilities and an upper limit for a $B(E2)$ value associated with decays from the shape isomer ^{236m}U to known states in ^{236}U have been determined. Branching ratios for the decay of a 0^+ level are included in the analysis. Details of the γ decay branches are illustrated in the decay scheme presented in Fig. 17, while the branching ratio for delayed fission is discussed in Sec. 7. Additionally, an upper limit of $< 10\%$ for a potential α-decay branch from the shape isomer has been adopted, based on the findings of Ref. [1].

For the two transitions identified in cascades 2 and 3 (see Table 2), which populate the 1^- states at 688 keV and 967 keV, $B(E1)$ values of 6.58×10^{-11} e^{2}fm^2 and 1.71×10^{-10} e^{2}fm^2 were obtained, respectively. These values are consistent with the range reported in Ref. [1], which found $B(E1)$ strengths between 3.16×10^{-11} and 3.16×10^{-10} e^{2}fm^2.

Furthermore, an improved upper limit has been established for the possible direct $E2$ transition to the first excited 2^+ state. The $B(E2)$ value for the $0^+ \rightarrow 2^+$ transition is constrained to $B(E2) < 6.76 \times 10^{-7}$ e^{2}fm^4, which is approximately a factor of three lower than the previously reported limit of $B(E2) < 2.0 \times 10^{-6}$ e^{2}fm^4 from Ref. [1].

The missing single-step γ decay of ^{236m}U can be compared to a previous γ decay measurement of the shape isomer ^{238m}U [2]. In that case, two γ transitions were observed: the dominant one at $E_\gamma = 2514$ keV, with a cross section of $\sigma = 90 \pm 25$ μb, was attributed to a direct transition from the second minimum to the 2^+ rotational state at 45 keV in the first minimum. A second transition at $E_\gamma = 1879$ keV, with $\sigma = 40 \pm 20$ μb, corresponds to a cascade similar to that observed in the present experiment, which feeds a 1^- state at 688 keV in ^{236}U.

While the Crystal Ball's high efficiency and excellent timing resolution made it uniquely suited to detect such rare decay processes, its limited energy resolution – typical for NaI detectors – poses a challenge for precise γ spectroscopy. This is particularly problematic for actinide nuclei, where excited states are closely spaced in energy. Future investigations will benefit from high-purity germanium (HPGe) detector arrays, which offer dramatically improved energy resolution. Although this would enhance sensitivity by approximately a factor of 50, it comes at the cost of significantly reduced photopeak efficiency. Even the most efficient HPGe arrays achieve only about 10% efficiency, which reduces the probability of detecting all γ transitions with their full energies for prompt and delayed cascades by a factor of ~ 1300 compared to NaI-based systems.

Additional limitations of HPGe detectors, such as inferior timing resolution and susceptibility to neutron-induced damage, present further challenges. A promising intermediate solution is the use of $LaBr_3$(Ce) scintillation detectors. These materials offer superior energy resolution (3–4% FWHM at 662 keV), high photoelectron yields, and improved detection efficiencies compared to NaI, making them well-suited for future studies of isomeric decay in heavy nuclei.

In summary, the refined investigation of the shape isomer ^{236m}U stays of significant interest for two principal reasons. First, the number of known shape isomers that deexcite from the second to the first potential minimum via γ decay remains extremely limited. Such isomers are expected in light actinide nuclei, particularly in the thorium and uranium regions, where γ decay can more effectively compete with delayed fission. This scenario is further complicated by the scarcity of suitable target-projectile combinations in this mass region that can populate states near or just below the fission barrier with appreciable cross sections. Moreover, the typically small branching ratios for γ decay relative to prompt fission, combined with the dominant population of states in the first minimum, impose substantial experimental challenges.

Second, the ^{236}U shape isomer provides a rare opportunity to test modern theoretical approaches describing the transition between superdeformed and normal-deformed nuclear configurations. Theoretical frameworks that have successfully described the decay of superdeformed high-spin states to normal-deformed configurations in nuclei such as ^{152}Dy and ^{194}Hg could potentially be extended to this low-spin, low-energy regime. For a comprehensive review of the population and γ decay of superdeformed nuclei, see Ref. [32]. In those cases, the superdeformed states couple weakly to one or more nearby normal-deformed states via small normal-deformed admixtures in their wave functions and quantum tunneling through the separating barrier allows the γ decay with huge hindrance factors.

In contrast, the excitation energy of ^{236m}U lies lower than in most cases of the $A \sim 150$ and $A \sim 190$ regions, and the decay occurs at very low spins – presumably even at the ground state of the second minimum. It is therefore compelling to investigate how the outcome of these calculations compare with the experimental results of several direct transitions with tiny B(E1) values depopulating the shape isomer ^{236m}U.

Acknowledgements The authors P.T. and P.R. gratefully acknowledge the support of O. Koschorrek and H. Krieger in the preparation of the detectors and experimental setup prior to the beam time. We also thank H. von Busch, Ch. Ender, J. B. Fitzgerald, F. Köck, T. Härtling, F. Heller, S. Schwebel, and A. Wiswesser for their valuable assistance during the extended duration of the experiment.

Funding Open Access funding enabled and organized by Projekt DEAL.

Data Availability Statement Data will be made available on reasonable request. [Authors' comment: The datasets generated during and/or analysed during the current study are available from the corresponding author on reasonable request.]

Code Availability Statement Code/software will be made available on reasonable request. [Authors' comment: The code/software generated during and/or analysed during the current study is available from the corresponding author on reasonable request.]

References

1. J. Schirmer, J. Gerl, D. Habs, D. Schwalm, Decay of the superdeformed shape isomer in ^{236}U. Phys. Rev. Lett. **63**(20), 2196–2199 (1989)
2. P.A. Russo, J. Pedersen, R. Vandenbosch, Gamma decay of the ^{238}U shape isomer. Nucl. Phys. Sect. A **240**(1), 13–28 (1975)
3. S.M. Polikhanov et al., Spontaneous fission with an anomalously short period. Sov. Phys. JETP **15**, 1016 (1962)
4. V.M. Strutinsky, Shell effects in nuclear masses and deformation energies. Nucl. Phys. A **95**(2), 420–442 (1967)
5. S. Bjørnholm, J.E. Lynn, The double-humped fission barrier. Rev. Mod. Phys. **52**(4), 725–931 (1980)
6. V. Metag, Systematics of fission isomer half-lives. Nucleonica **20**, 2096 (1970)
7. Z. Ren, X. Chang, Spontaneous fission half-lives of heavy nuclei in ground state and in isomeric state. Nucl. Phys. A **759**(1), 64–78 (2005)
8. P. Møller, A.J. Sierk, T. Ichikawa, A. Iwamoto, R. Bengtsson, H. Uhrenholt, S. Aberg, Heavy-element fission barriers. Phys. Rev. C **79**, 064304 (2009)
9. H. Abusara, A.V. Afanasjev, P. Ring, Fission barriers in actinides in covariant density functional theory: the role of triaxiality. Phys. Rev. C **82**, 044303 (2010)
10. H.J. Specht, J. Weber, E. Konecny, D. Heunemann, Identification of a rotational band in the ^{240}Pu fission isomer. Phys. Lett. B **41**(1), 43–46 (1972)
11. V. Metag, D. Habs, H.J. Specht, Spectroscopic properties of fission isomers. Phys. Rep. **65**(1), 1–41 (1980)
12. P.G. Thirolf, D. Habs, Spectroscopy in the second and third minimum of actinide nuclei. Prog. Part. Nucl. Phys. **49**(2), 325–402 (2002)
13. R. Repnow, V. Metag, J.D. Fox, P. Von Brentano, Evidence for a direct reaction mechanism in the production of fission isomers. Nucl. Phys. A **147**(1), 183–192 (1970)
14. K.L. Wolf, R. Vandenbosch, P.A. Russo, M.K. Mehta, C.R. Rudy, Spontaneous fission isomerism in uranium isotopes. Phys. Rev. C **1**, 2096–2101 (1970)
15. J. Pedersen, B. Rasmussen, An investigation of the population of the shape isomer ^{236m}U through the (d, p) reaction. Nucl. Phys. A **178**(2), 449–457 (1972)
16. J. Christiansen, G. Hempel, H. Ingwersen, W. Klinger, G. Schatz, W. Witthuhn, Investigation of delayed fission in ^{236}U. Nucl. Phys. A **239**(2), 253–259 (1975)
17. S. Zhu, Nuclear data sheets for A=236. Nucl. Data Sheets **182**, 2–129 (2022)
18. J. Balibrea-Correa, E. Mendoza, D. Cano-Ott, E. González, R. Capote et al., Measurement of the α ratio and (n, γ) cross section of ^{235}U from 0.2 to 200 eV at n-TOF. Phys. Rev. C **102**, 044615 (2020)
19. J. Borggreen, J. Pedersen, G. Sletten, R. Heffner, E. Swanson, The rotational band of the ^{236}U shape isomer. Nucl. Phys. A **279**(2), 189–198 (1977)
20. H. Bartsch, W. Guenther, K. Huber, U. Kneissl, H. Krieger, H.J. Maier, Search for a gamma-decay of the ^{236}U shape isomer. Nucl. Phys. A **306**(1), 29–37 (1978)
21. W. Günther, K. Huber, U. Kneissl, H. Krieger, Population of the ^{236}U shape isomer in a photonuclear reaction. Nucl. Phys. Sect. A **297**(2), 254–262 (1978)
22. V. Metag, D. Habs, K. Helmer, U.V. Helmolt, H.W. Heyng, B. Kolb, D. Pelte, D. Schwalm, W. Hennerici, H.J. Hennrich, G. Himmele, E. Jaeschke, R. Repnow, W. Wahl, R.S. Simon, R. Albrecht, The Darmstadt Heidelberg crystal ball, in *Detectors in Heavy-Ion Reactions*, ed. by W. von Oertzen, pp. 163–178 (1983). Springer, Berlin
23. R. Müller, A.A. Naqvi, F. Käppeler, F. Dickmann, Fragment velocities, energies, and masses from fast neutron induced fission of ^{235}U. Phys. Rev. C **29**(3), 885 (1984)
24. Ch. Straede, C. Budtz-Jørgensen, H.H. Knitter, ^{235}U(n, f) fragment mass-, kinetic energy- and angular distributions for incident neutron energies between thermal and 6 MeV. Nucl. Phys. A **462**, 85–108 (1987)
25. J.L. Sida, P. Armbruster, M. Bernas, J.P. Bocquet, R. Brissot, H.R. Faust, Mass, charge, and energy distributions in very asymmetric thermal fission of ^{235}U. Nucl. Phys. A **502**, 233–242 (1989)
26. N.L. Lark, G. Sletten, J. Pedersen, S. Bjørnholm, Spontaneously fissioning isomers in U, Np, Pu and Am isotopes. Nucl. Phys. A **139**(3), 481–500 (1969)
27. H.C. Britt, B.H. Erkkila, Population of fission isomers in ^{236}U by the (d, p) reaction. Phys. Rev. C **4**, 1441–1443 (1971)
28. U. Goerlach, D. Habs, V. Metag, B. Schwartz, H.J. Specht, H. Backe, Lowest β-vibrational phonon in the second minima of ^{236,238}U. Phys. Rev. Lett. **48**, 1160–1163 (1982)
29. U. Goerlach, Intermediäre Struktur in der prompten und verzögerten Spaltung von ^{236}U und ^{240}Pu
30. J. Margraf, A. Degener, H. Friedrichs, R.D. Heil, A. Jung, U. Kneissl, S. Lindenstruth, H.H. Pitz, H. Schacht, U. Seemann, R. Stock, C. Wesselborg, P. von Brentano, A. Zilges, Photoexcitation of low-lying dipole transitions in ^{236}U. Phys. Rev. C **42**, 771–774 (1990)
31. V. Andersen, C.J. Christensen, J. Borggreen, The shape isomer in ^{236}U populated by thermal neutron capture. Nucl. Phys. A **269**(2), 338–348 (1976)
32. A. Lopez-Martens, T. Lauritsen, S. Leoni, T. Døssing, T.L. Khoo, S. Siem, Population and decay of superdeformed nuclei probed by discrete and quasi-continuum γ-ray spectroscopy. Prog. Part. Nucl. Phys. **89**, 137–186 (2016)